Origin of Perpendicular Magnetic Anisotropy and Large Orbital Moment in Fe Atoms on MgO

S. Baumann,[1,2] F. Donati,[3] S. Stepanow,[4] S. Rusponi,[3] W. Paul,[1] S. Gangopadhyay,[1,5] I. G. Rau,[1]
G. E. Pacchioni,[3] L. Gragnaniello,[3] M. Pivetta,[3] J. Dreiser,[3,6] C. Piamonteze,[6] C. P. Lutz,[1]
R. M. Macfarlane,[1] B. A. Jones,[1] P. Gambardella,[4] A. J. Heinrich,[1] and H. Brune[3]

[1]*IBM Almaden Research Center, 650 Harry Road, San Jose, California 95120, USA*
[2]*Department of Physics, University of Basel, Klingelbergstrasse 82, CH-4056 Basel, Switzerland*
[3]*Institute of Condensed Matter Physics, École Polytechnique Fédérale de Lausanne (EPFL), Station 3,
CH-1015 Lausanne, Switzerland*
[4]*Department of Materials, ETH Zürich, Hönggerbergring 64, CH-8093 Zürich, Switzerland*
[5]*Department of Physics, University of California, Davis, California 95616, USA*
[6]*Swiss Light Source (SLS), Paul Scherrer Institute (PSI), CH-5232 Villigen PSI, Switzerland*

We report on the magnetic properties of individual Fe atoms deposited on MgO(100) thin films probed by x-ray magnetic circular dichroism and scanning tunneling spectroscopy. We show that the Fe atoms have strong perpendicular magnetic anisotropy with a zero-field splitting of 14.0 ± 0.3 meV/atom. This is a factor of 10 larger than the interface anisotropy of epitaxial Fe layers on MgO and the largest value reported for Fe atoms adsorbed on surfaces. The interplay between the ligand field at the O adsorption sites and spin-orbit coupling is analyzed by density functional theory and multiplet calculations, providing a comprehensive model of the magnetic properties of Fe atoms in a low-symmetry bonding environment.

The Fe/MgO(100) interface is a fundamental building block of spintronic devices. Several key properties for the realization of magnetic tunnel junctions, such as perpendicular magnetic anisotropy (PMA) [1–4], giant tunnel magnetoresistance [5–8], and electric field control of the magnetization [9–11] are realized at once in this system. The origin of the interfacial PMA in Fe/MgO layers has been widely discussed [2,10–13]. According to recent first principles calculations, PMA results from a combination of both interface and "bulk" effects, in which the hybridization between Fe-$3d$ and O-$2p$ orbitals [2], the Fe thickness [12], and the bcc-like layer stacking of the magnetic layer [13] play a substantial role. Experimental studies of the Fe/MgO interface, however, usually start from Fe films with a thickness larger than 2 to 3 monolayers (ML) and uneven morphology [1,14–16], which makes it difficult to isolate purely interfacial effects and, in particular, the influence of the orbital hybridization between Fe and MgO on the magnetic moment and anisotropy.

This limitation can be overcome by studying isolated Fe atoms deposited on MgO thin films, for which, as will be shown in this Letter, the magnetic properties are uniquely determined by the Fe-MgO interaction. Previous works have only focused on Fe atoms diluted in bulk MgO since they have long been considered as a model system for studying the interplay of crystal field, spin-orbit coupling (SOC), and magnetic moment on the low energy excitation spectra of transition-metal impurities in insulators [17–19]. However, they have never been investigated at the surface, where the local symmetry is drastically altered with respect to the octahedral environment found inside MgO crystals and can potentially enhance the anisotropy energy, as similarly observed in previous studies of adatoms on nonmagnetic surfaces [20–28].

Here, we report a study of the magnetic properties of isolated Fe atoms on MgO thin films on Ag(100) performed by x-ray magnetic circular dichroism (XMCD), inelastic electron tunneling spectroscopy (IETS), multiplet calculations, and density functional theory (DFT). We show that Fe atoms preferentially bind to O surface sites and develop strong PMA as a result of the interplay between the low-symmetry ligand field and SOC at these sites. Our IETS measurements reveal a PMA with a zero-field splitting of 14 meV and a corresponding total anisotropy barrier of 18 meV/atom, one order of magnitude larger with respect to the interfacial anisotropy reported in Fe/MgO blanket layers [1,2,13,15]. Our analysis reveals that the first-order orbital moment of Fe is quenched by the weak fourfold ligand field due to the Mg atoms and relates the PMA to the unusually large second-order orbital moment induced by SOC at the Fe sites. These results shed light on the interfacial nature of PMA in Fe/MgO and demonstrate the potential of MgO substrates to provide a low-symmetry bonding geometry for magnetic atoms, similar to that encountered in axial molecular magnets [29,30].

Figure 1(a) shows a STM image of two individual Fe atoms deposited at ≈ 8 K on 1 ML MgO(100) grown on Ag(100) [31–34]. At the Fe coverages of 0.01–0.03 ML
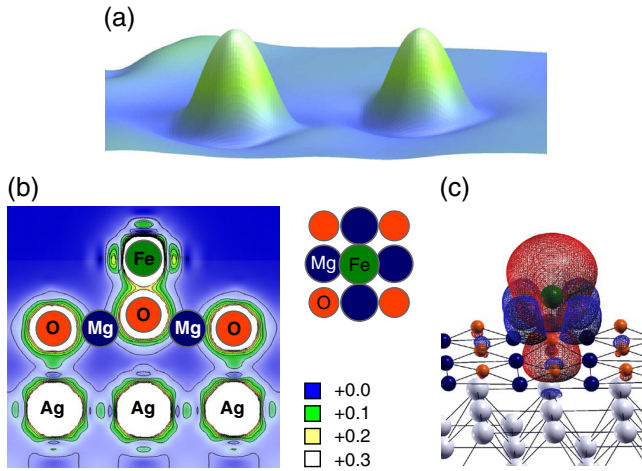
FIG. 1 (color online).   (a) STM image of two Fe atoms on a ML MgO(100) grown on Ag(100) (4 nm × 4 nm, tunnel current $I_t = 5$ pA, tunnel voltage $V_t = 100$ mV). (b) Side view of DFT-calculated binding geometry and charge density [color scale, $1e/(\text{au})^3$; Fe, green; O, red; Mg, blue]. (Middle sketch) Top view ball model of the binding geometry. (c) Oblique view of DFT-calculated valence electron spin density contours (positive spin polarization, red; negative, blue).

[one ML is defined as one Fe atom per MgO(100) unit cell] used in the present study, we observe isolated Fe atoms rather than clusters. We find only one Fe species with an apparent height of 180 pm. Using DFT with the generalized gradient approximation and on-site Coulomb interactions ($U = 3.2$ eV) [52] for the Fe d states, we find the on-top oxygen adsorption site to be the lowest in energy [32,34]. Figure 1(b) reveals that the O beneath Fe is displaced by 40 pm upwards from the MgO plane, indicating a strong Fe–O bond. A significant fraction of charge is transferred to the O atom, resulting in an overall positive charge of $+0.44\,e$ on the Fe [34].

For an Fe atom on 1 ML MgO/Ag(100), DFT calculations predict a spin moment of 3.7 μ_B. The majority spin density, shown in red in Fig. 1(c), is mostly axially symmetric. The induced polarization of the underneath O atom slightly increasing the overall spin moment to 3.8 μ_B. The fourfold symmetry of the binding site shows up strongly in the minority spin density (blue) with a characteristic four-lobed shape. This is in contrast to Co, the closest 3d element, which exhibits nearly perfect axial spin density on the MgO surface [28]. The calculated spin of the Fe atom is unchanged on 2 ML MgO/Ag(100), suggesting that its value does not depend on the MgO thickness. This facilitates the interpretation of synchrotron measurements on samples having several coexisting MgO thicknesses [34].

To access the magnetic properties of Fe atoms, we performed XMCD measurements at the EPFL/PSI X-Treme beam line of the Swiss Light Source [53]. X-ray absorption spectra (XAS) and the resulting XMCD signal are shown in Figs. 2(a) and 2(b) (see Ref. [34] for the
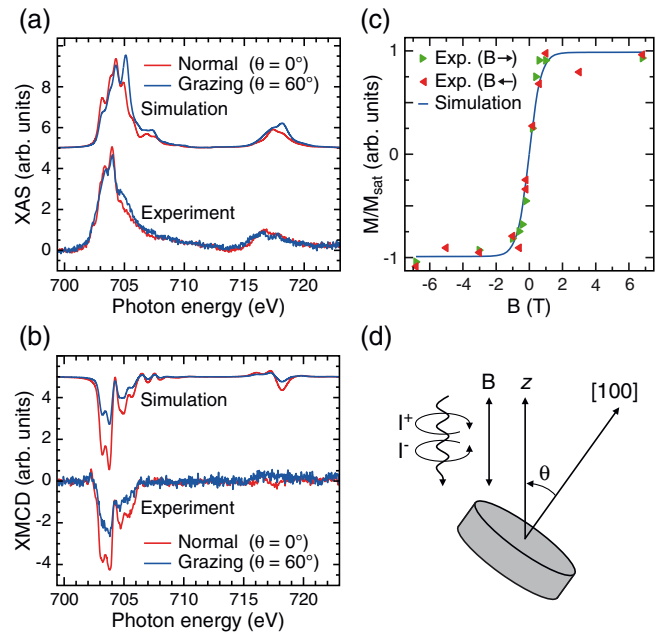

FIG. 2 (color online).   (a) Measured and simulated XAS over the Fe L_3 and L_2 edges for 0.03 ML Fe on a MgO film on Ag(100) with an average thickness of 3 ML ($T = 2.5$ K, $B = 6.8$ T, incident angle θ, total electron yield mode). (b) XMCD spectra for both geometries. (c) Out-of-plane magnetization curve measured by first saturating the sample at 6.8 T (red) and −6.8 T (green) and then moving to the respective field value ($T = 2.5$ K). The values of the magnetization are obtained from the maximum of the XMCD signal at 704 eV. The solid line represents $\langle 2S_z(B)\rangle + \langle L_z(B)\rangle$ determined by the multiplet fit with a saturation moment of 5.2 μ_B. (d) Sketch of the measurement geometry. The magnetic field is aligned to the incident beam.

experimental details). The Fe L_3 and L_2 edges exhibit sharp multiplet structures characteristic of an ensemble of single adatoms on identical adsorption sites [54]. The XMCD signal is larger at normal than at grazing incidence, revealing a PMA in Fe atoms on MgO.

More insight into the magnetic levels and the evolution of their energies is gained from multiplet theory [55]. The calculated spectra shown in Fig. 2 are in good agreement with the experiment for both incident beam directions. In addition, the experimental out-of-plane magnetization curve in Fig. 2(c) is well reproduced by the line showing the out-of-plane projected field-dependent total magnetic moment $\langle 2S_z(B)\rangle + \langle L_z(B)\rangle$ derived from multiplet calculations. In these calculations we included charge transfer to the O ligand, leading to configuration mixing, the axial ligand field due to the nearest-neighbor O atom (Ds and Dt), the cubic distortion due to the four next-nearest-neighbor Mg atoms (Dq), SOC (ζ), and the external magnetic field (B). Best agreement is obtained with a 90% $d^6 + 10\%\ d^7l$ configuration of the Fe atom, where l refers to a ligand hole in the neighboring O atom.

The configuration mixing and the axial terms Ds and Dt result in a tenfold degenerate ground state
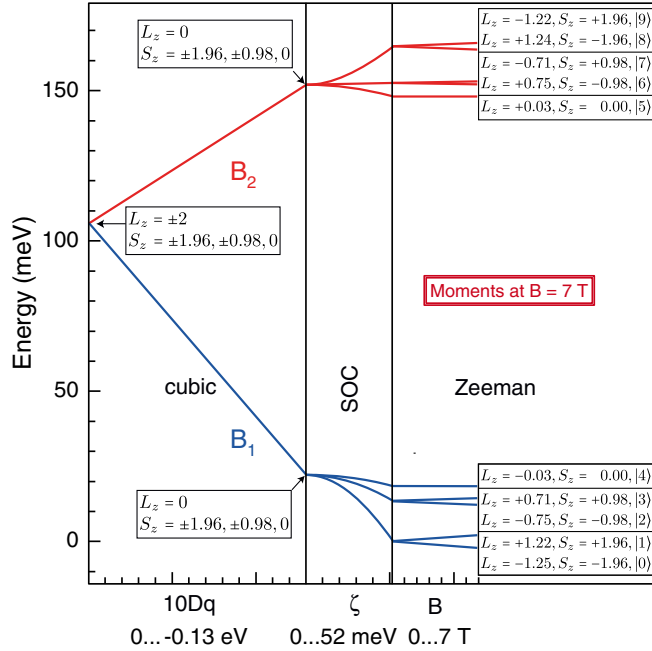
FIG. 3 (color online).   Energy level diagram resulting from the multiplet simulation of the XAS and XMCD spectra (for the full diagram, see Ref. [34]). The S_z and L_z values in the labels are the respective expectation values; the $\langle\rangle$ signs have been omitted for brevity. The cubic crystal field quenches the orbital moment and creates two spin quintuplets with B_1 and B_2 symmetry, which are both further separated by the SOC and the Zeeman energy. Labels $|0\rangle$–$|4\rangle$ and $|5\rangle$–$|9\rangle$ denote the states deriving from the B_1 and B_2 quintuplets, respectively.

$(\langle L_z \rangle = \pm 2) \otimes (\langle S_z \rangle = \pm 1.96, \pm 0.98, \text{and} 0)$ [34]. Figure 3 illustrates its evolution under the action of Dq, ζ, and B. The cubic term Dq strongly perturbs the lowest multiplet and creates two spin quintuplets with fully quenched orbital moments, $(\langle L_z \rangle = 0) \otimes (\langle S_z \rangle = \pm 1.96, \pm 0.98, \text{and} 0)$. The SOC splits the lowest quintuplet with B_1 symmetry (blue) into essentially three energy levels, and restores more than half of the free-atom orbital moment by coupling the two lowest orbital levels in a second-order perturbation [56]. The combined effect of the ligand field and SOC lowers the energy of the states with the largest $|S_z|$ components and, therefore, engenders a PMA in Fe atoms.

The out-of-plane magnetic field lifts the remaining degeneracy of the five states labeled $|0\rangle$–$|4\rangle$. At 6.8 T, the new ground state $|0\rangle$ exhibits large orbital $\langle L_z \rangle \mu_B = 1.25\,\mu_B$ and spin magnetic moments $2\langle S_z \rangle \mu_B = 3.92\,\mu_B$, in good agreement with results obtained from DFT calculations [34]. In contrast, the excited spin quintuplet (red) has B_2 symmetry, lies ≈ 100 meV higher in energy, and has its orbital and spin magnetic moments antialigned. This results in smaller total magnetic moments and hence a smaller Zeeman splitting.

Our IETS measurements on individual Fe atoms determine the energy splitting of the lowest magnetic states with high precision, and they thereby complement XMCD.
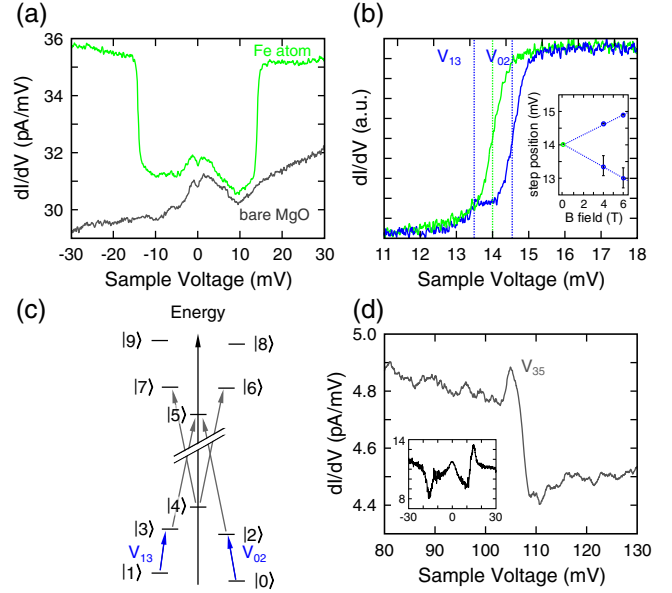

FIG. 4 (color online). (a) STM differential conductance (dI/dV) spectrum on Fe/1 ML MgO(100)/Ag(100); dI/dV on bare MgO is shown for comparison ($T = 0.6$ K, $B = 0$ T, modulation with $V_{mod} = 150\,\mu$V rms at $f = 806$ Hz, set point before opening the feedback loop $I_t = 1$ nA, $V_t = 30$ mV). (b) Positive conductance step at out-of-plane fields of 0 T (green) and 4 T (blue). (Inset) Field splitting of step energies. (c) Sketch of the magnetic states and the allowed IETS excitations. (d) IETS feature corresponding to the superposition of V_{35}, V_{25}, V_{47}, and V_{46}, measured with a spin-polarized tip ($T = 1.2$ K, $B = 2$ T, $V_{mod} = 1.5$ mV, $I_t = 1$ nA, $V_t = 100$ mV). (Inset) Spin-polarized spectrum in the same energy window as (a). Jagged edges at the conductance steps originate from the superposition of inelastic spin excitations and spin pumping, and they reveal that the tip is magnetic.

Figure 4(a) displays clear conductance steps with 15% amplitude located at $\pm 14.0 \pm 0.3$ mV at zero field (the error bar refers to variations between atoms at different locations of the MgO film). The magnetic nature of the underlying inelastic excitations is demonstrated by the splitting of the excitation energy in an out-of-plane magnetic field shown in Fig. 4(b). For in-plane fields the splitting is absent [34], confirming the strong PMA.

Connection between the transitions excited in IETS and the states derived from the multiplet calculations is established by the level diagram shown in Fig. 4(c). The blue arrows indicate the first two excitations possible for tunnel electrons, $|0\rangle \rightarrow |2\rangle$ and $|1\rangle \rightarrow |3\rangle$, with the corresponding tunneling voltages labeled V_{02} and V_{13}. Within the lowest multiplet, only these excitations fulfill the spin selection rule $\Delta S_z = 0, \pm 1$ [21]. They correspond to the conductance steps in Figs. 4(a) and 4(b). At zero field, the value $V_{02} = V_{13} = 14.0$ mV corresponds to the zero-field splitting of the ground and first excited doublets. This is in excellent agreement with the level separation of 13 meV found in the multiplet calculations.

These excitations split symmetrically in an external out-of-plane field; see Fig. 4(b). The amplitude of V_{13} is significantly smaller than that of V_{02} because the corresponding transition starts from the excited state $|1\rangle$. The fact that V_{13} is visible implies that the tunnel current drives the occupation of the $|1\rangle$ state, and that its lifetime is longer than the mean time between tunneling electrons of the order of 1 ns [57].

As seen in the inset of Fig. 4(b), the splitting is linear and its slope indicates an effective g^* value of 2.57 ± 0.06 in the z direction. This is significantly above the free-electron value of $g_e = 2$ and thus confirms the presence of a large orbital magnetic moment for Fe on MgO [58,59]. The latter evidence is independently supported by the large orbital-to-effective-spin ratio 0.71 ± 0.08 derived from sum rules [34,60–62]. This value is obtained by the experimental XMCD only and even slightly exceeds the calculated ratio of 0.59 from the multiplet analysis. Although first-order unquenched orbital moments were observed in Fe-based linear molecules [29,30], a value larger than 1 μ_B/atom, as observed in the present experiment, is exceptional for second-order SOC [18,63].

The splitting of the lowest fivefold multiplet, being due to the second-order SOC, can be described using a conventional spin Hamiltonian with a quadratic anisotropy term DS_z^2, where $D = -4.7$ meV is the uniaxial anisotropy parameter. This approach is widely used to interpret the magnetic IETS excitations of adatoms [21,26,64] and molecules [65] at the surface. However, the use of STM measurements solely does not guarantee an unambiguous determination of S and, therefore, of the total anisotropy barrier. In our analysis, we circumvent this issue by combining IETS and XMCD. The first measures the zero-field splitting directly and very precisely, while the second identifies the ground and excited states with their spin and orbital magnetic moments, as well as their angular anisotropies. Using the value of $S = 2$ obtained from XMCD and the zero-field splitting of 14 meV measured with IETS, we estimate a total anisotropy barrier of $|DS_z^2| = 18.8$ meV, in excellent agreement with the value of 18.3 meV obtained by the energy separation between the $|0\rangle, |1\rangle$ states and the $|4\rangle$ singlet from the multiplet analysis. The total anisotropy barrier of Fe atoms on MgO is, therefore, strongly enhanced with respect to Fe films on MgO [1,2,13–16] due to the reduced in-plane coordination of the Fe atoms [23]. Remarkably, it is more than twice the largest value reported for individual Fe atoms adsorbed on other surfaces [21,66–68] and embedded in bulk MgO [17–19], and the barrier approaches that reported for Fe atoms in linear molecules [30].

The magnetic properties of Fe are quite different from those of Co, which shows an unquenched first-order orbital moment and record-high PMA on the MgO surface [28]. This is a consequence of the orbital symmetry of the corresponding magnetic states. In a fourfold symmetric ligand field, the fourth-order cubic term Dq combines orbital states separated by $\Delta L_z = \pm 4$. This allows the mixing of the Fe states with $L_z = \pm 2$, with the consequent formation of states with a quenched first-order orbital moment. In contrast, Co has $L_z = \pm 3$ and is protected from such mixing; thus, it exhibits a ground state orbital moment largely unchanged with respect to the free atom, together with a maximum first-order SOC splitting of 58 meV [28].

Spin-polarized STM tips reveal an additional conductance step at ≈ 105 mV; see Fig. 4(d). Since this step is absent for nonpolarized tips, we assign it to an electron driven occupation change of the magnetic states at the respective threshold energies (spin pumping). In agreement with this assignment, the step height depends on the set-point current, as the tunneling electrons must arrive frequently enough to probe the excited states before they decay [57]. According to the spin selection rule, we can assign the ≈ 105 mV step to the four transitions V_{35}, V_{25}, V_{46}, and V_{47} that are very close in energy [69]. The multiplet calculations estimate $V_{35} \approx 134$ meV, in reasonable agreement with the one directly probed by STM. This confirms the validity of the multiplet model on a scale of more than 100 meV, the largest ever probed by IETS. Transitions between states belonging to different spin multiplets have been observed in spin chains [57,70] and molecular magnets [71]. Unique to Fe on MgO, the excitation from lower to upper spin multiplets involves a transition from aligned (lower multiplet) to antialigned (upper multiplet) orbital and spin moments.

In conclusion, the present study reveals how the large PMA and orbital moment of Fe atoms on MgO arise from the interplay between SOC and low-symmetry ligand field of the O adsorption site. Our analysis, going beyond the spin-Hamiltonian approach, allows us to follow the effect of each interaction on the quantum levels of a magnetic system, and proves to be an effective approach to understand and engineer the properties of atomic-scale tunnel magnetoresistance junctions.

---

[1] M. Klaua, D. Ullmann, J. Barthel, W. Wulfhekel, J. Kirschner, R. Urban, T. L. Monchesky, A. Enders, J. F. Cochran, and B. Heinrich, Phys. Rev. B **64**, 134411 (2001).

[2] H. X. Yang, M. Chshiev, B. Dieny, J. H. Lee, A. Manchon, and K. H. Shin, Phys. Rev. B **84**, 054401 (2011).

[3] S. Ikeda, K. Miura, H. Yamamoto, K. Mizunuma, H. D. Gan, M. Endo, S. Kanai, J. Hayakawa, F. Matsukura, and H. Ohno, Nat. Mater. **9**, 721 (2010).

[4] M. Cubukcu, O. Boulle, M. Drouard, K. Garello, C. O. Avci, I. M. Miron, J. Langer, B. Ocker, P. Gambardella, and G. Gaudin, Appl. Phys. Lett. **104**, 042406 (2014).

[5] J. Mathon and A. Umerski, Phys. Rev. B **63**, 220403 (2001).

[6] W. H. Butler, X.-G. Zhang, T. C. Schulthess, and J. M. MacLaren, Phys. Rev. B **63**, 054416 (2001).

[7] S. Yuasa, T. Nagahama, A. Fukushima, Y. Suzuki, and K. Ando, Nat. Mater. **3**, 868 (2004).

[8] S. S. P. Parkin, C. Kaiser, A. Panchula, P. M. Rice, B. Hughes, M. Samant, and S. H. Yang, Nat. Mater. **3**, 862 (2004).

[9] T. Maruyama, Y. Shiota, T. Nozaki, K. Ohta, N. Toda, M. Mizuguchi, A. A. Tulapurkar, T. Shinjo, M. Shiraishi, S. Mizukami, Y. Ando, and Y. Suzuki, Nat. Nanotechnol. **4**, 158 (2009).

[10] K. Nakamura, T. Akiyama, T. Ito, M. Weinert, and A. J. Freeman, Phys. Rev. B **81**, 220409 (2010).

[11] M. K. Niranjan, C.-G. Duan, S. S. Jaswal, and E. Y. Tsymbal, Appl. Phys. Lett. **96**, 222504 (2010).

[12] A. Hallal, H. X. Yang, B. Dieny, and M. Chshiev, Phys. Rev. B **88**, 184423 (2013).

[13] K. Hotta, K. Nakamura, T. Akiyama, T. Ito, T. Oguchi, and A. J. Freeman, Phys. Rev. Lett. **110**, 267206 (2013).

[14] C. Martínez Boubeta, C. Clavero, J. M. García-Martín, G. Armelles, A. Cebollada, L. Balcells, J. L. Menéndez, F. Peiró, A. Cornet, and M. F. Toney, Phys. Rev. B **71**, 014407 (2005).

[15] C.-H. Lambert, A. Rajanikanth, T. Hauet, S. Mangin, E. E. Fullerton, and S. Andrieu, Appl. Phys. Lett. **102**, 122410 (2013).

[16] J. Okabayashi, J. W. Koo, H. Sukegawa, S. Mitani, Y. Takagi, and T. Yokoyama, Appl. Phys. Lett. **105**, 122408 (2014).

[17] F. S. Ham, W. M. Schwarz, and M. C. M. O'Brien, Phys. Rev. **185**, 548 (1969).

[18] T. Haupricht, R. Sutarto, M. W. Haverkort, H. Ott, A. Tanaka, H. H. Hsieh, H. J. Lin, C. T. Chen, Z. Hu, and L. H. Tjeng, Phys. Rev. B **82**, 035120 (2010).

[19] A. Ferrón, F. Delgado, and J. Fernández-Rossier, New J. Phys. **17**, 033020 (2015).

[20] P. Gambardella, S. Rusponi, M. Veronese, S. S. Dhesi, C. Grazioli, A. Dallmeyer, I. Cabria, R. Zeller, P. H. Dederichs, K. Kern, C. Carbone, and H. Brune, Science **300**, 1130 (2003).

[21] C. F. Hirjibehedin, C. Y. Lin, A. F. Otte, M. Ternes, C. P. Lutz, B. A. Jones, and A. J. Heinrich, Science **317**, 1199 (2007).

[22] F. Meier, L. Zhou, J. Wiebe, and R. Wiesendanger, Science **320**, 82 (2008).

[23] H. Brune and P. Gambardella, Surf. Sci. **603**, 1812 (2009).

[24] S. Loth, S. Baumann, C. P. Lutz, D. M. Eigler, and A. J. Heinrich, Science **335**, 196 (2012).

[25] A. A. Khajetoorians, B. Baxevanis, C. Hübner, T. Schlenk, S. Krause, T. O. Wehling, S. Lounis, A. Lichtenstein, D. Pfannkuche, J. Wiebe, and R. Wiesendanger, Science **339**, 55 (2013).

[26] F. Donati, Q. Dubout, G. Autès, F. Patthey, F. Calleja, P. Gambardella, O. V. Yazyev, and H. Brune, Phys. Rev. Lett. **111**, 236801 (2013).

[27] F. Donati, L. Gragnaniello, A. Cavallin, F. D. Natterer, Q. Dubout, M. Pivetta, F. Patthey, J. Dreiser, C. Piamonteze, S. Rusponi, and H. Brune, Phys. Rev. Lett. **113**, 177201 (2014).

[28] I. G. Rau, S. Baumann, S. Rusponi, F. Donati, S. Stepanow, L. Gragnaniello, J. Dreiser, C. Piamonteze, F. Nolting, S. Gangopadhyay, O. R. Albertini, R. Macfarlane, C. P. Lutz, B. A. Jones, P. Gambardella, A. J. Heinrich, and H. Brune, Science **344**, 988 (2014).

[29] W. M. Reiff, A. M. LaPointe, and E. H. Witten, J. Am. Chem. Soc. **126**, 10206 (2004).

[30] J. M. Zadrozny, D. J. Xia, M. Atanasov, G. J. Long, F. Grandjean, F. Neese, and J. R. Long, Nat. Chem. **5**, 577 (2013).

[31] S. Schintke, S. Messerli, M. Pivetta, F. Patthey, L. Libioulle, M. Stengel, A. De Vita, and W. D. Schneider, Phys. Rev. Lett. **87**, 276801 (2001).

[32] K. Neyman, C. Inntam, V. Nasluzov, R. Kosarev, and N. Rösch, Appl. Phys. A **78**, 823 (2004).

[33] S. Baumann, I. G. Rau, S. Loth, C. P. Lutz, and A. J. Heinrich, ACS Nano **8**, 1739 (2014).

[34] See Supplemental Material at http://link.aps.org/supplemental/10.1103/PhysRevLett.115.237202, which includes Refs. [35–51], for details about the sample preparation, the STM and XMCD measurements, and the DFT and multiplet calculations.

[35] A. J. Heinrich, J. A. Gupta, C. P. Lutz, and D. M. Eigler, Science **306**, 466 (2004).

[36] R. C. Jaklevic and J. Lambe, Phys. Rev. Lett. **17**, 1139 (1966).

[37] J. S. Griffith, Phys. Rev. **132**, 316 (1963).

[38] P. Giannozzi et al., J. Phys. Condens. Matter **21**, 395502 (2009).

[39] P. Blaha, K. Schwarz, G. Madsen, D. Kvasnicka, and J. Luitz, WIEN2k: An Augmented Plane Wave + Local Orbitals Program for Calculating Crystal Properties (Karlheinz Schwarz, Technische Universität Wien, Vienna, 2001).

[40] M. Sgroi, C. Pisani, and M. Busso, Thin Solid Films **400**, 64 (2001).

[41] B. D. Yu, Phys. Rev. B **71**, 193403 (2005).

[42] O. R. Albertini, A. Y. Liu, and B. A. Jones, Phys. Rev. B **91**, 214423 (2015).

[43] M. S. S. Brooks, Physica (Amsterdam) **130B+C**, 6 (1985).

[44] O. Eriksson, B. Johansson, R. C. Albers, A. M. Boring, and M. S. S. Brooks, Phys. Rev. B **42**, 2707 (1990).

[45] C. O. Rodriguez, M. V. Ganduglia-Pirovano, E. L. Peltzer y Blancá, M. Petersen, and P. Novák, Phys. Rev. B **63**, 184413 (2001).

[46] A. Lehnert, S. Rusponi, M. Etzkorn, S. Ouazi, P. Thakur, and H. Brune, Phys. Rev. B **81**, 104430 (2010).

[47] C. T. Chen, Y. U. Idzerda, H.-J. Lin, N. V. Smith, G. Meigs, E. Chaban, G. H. Ho, E. Pellegrin, and F. Sette, Phys. Rev. Lett. **75**, 152 (1995).

[48] S. Stepanow, A. Mugarza, G. Ceballos, P. Moras, J. C. Cezar, C. Carbone, and P. Gambardella, Phys. Rev. B **82**, 014405 (2010).

[49] G. van der Laan and B. T. Thole, Phys. Rev. B **43**, 13401 (1991).

[50] O. Gunnarsson and K. Schönhammer, Phys. Rev. B **28**, 4315 (1983).

[51] A. Abragam and B. Bleaney, *Electron Paramagnetic Resonance of Transition Ions* (Clarendon Press, Oxford, 1986).

[52] M. Cococcioni and S. de Gironcoli, Phys. Rev. B **71**, 035105 (2005).

[53] C. Piamonteze, U. Flechsig, S. Rusponi, J. Dreiser, J. Heidler, M. Schmidt, R. Wetter, M. Calvi, T. Schmidt, H. Pruchova, J. Krempasky, C. Quitmann, H. Brune, and F. Nolting, J. Synchrotron Radiat. **19**, 661 (2012).

[54] P. Gambardella, S. S. Dhesi, S. Gardonio, C. Grazioli, P. Ohresser, and C. Carbone, Phys. Rev. Lett. **88**, 047202 (2002).

[55] F. de Groot, Chem. Rev. **101**, 1779 (2001).

[56] B. McGarvey, in *Transition Metal Chemistry*, Vol. 3, edited by R. L. Carlin and M. Dekker (John Wiley & Sons, New York, 1966).

[57] S. Loth, K. von Bergmann, M. Ternes, A. F. Otte, C. P. Lutz, and A. J. Heinrich, Nat. Phys. **6**, 340 (2010).

[58] B. Chilian, A. A. Khajetoorians, S. Lounis, A. T. Costa, D. L. Mills, J. Wiebe, and R. Wiesendanger, Phys. Rev. B **84**, 212401 (2011).

[59] T. Schuh, T. Balashov, T. Miyamachi, S. Y. Wu, C. C. Kuo, A. Ernst, J. Henk, and W. Wulfhekel, Phys. Rev. B **84**, 104401 (2011).

[60] B. T. Thole, P. Carra, F. Sette, and G. van der Laan, Phys. Rev. Lett. **68**, 1943 (1992).

[61] P. Carra, B. T. Thole, M. Altarelli, and X. Wang, Phys. Rev. Lett. **70**, 694 (1993).

[62] The ratio is defined as $\langle L_z \rangle / \langle 2S_z + 7T_z \rangle$, where $\langle T_z \rangle$ is the z-projected dipolar magnetic moment.

[63] J. Bartolomé, F. Bartolomé, L. M. García, G. Filoti, T. Gredig, C. N. Colesniuc, I. K. Schuller, and J. C. Cezar, Phys. Rev. B **81**, 195405 (2010).

[64] A. F. Otte, M. Ternes, K. von Bergmann, S. Loth, H. Brune, C. P. Lutz, C. F. Hirjibehedin, and A. J. Heinrich, Nat. Phys. **4**, 847 (2008).

[65] N. Tsukahara, K.-i. Noto, M. Ohara, S. Shiraki, N. Takagi, Y. Takata, J. Miyawaki, M. Taguchi, A. Chainani, S. Shin, and M. Kawai, Phys. Rev. Lett. **102**, 167203 (2009).

[66] A. A. Khajetoorians, S. Lounis, B. Chilian, A. T. Costa, L. Zhou, D. L. Mills, J. Wiebe, and R. Wiesendanger, Phys. Rev. Lett. **106**, 037205 (2011).

[67] A. A. Khajetoorians, T. Schlenk, B. Schweflinghaus, M. dos Santos Dias, M. Steinbrecher, M. Bouhassoune, S. Lounis, J. Wiebe, and R. Wiesendanger, Phys. Rev. Lett. **111**, 157204 (2013).

[68] G. E. Pacchioni, L. Gragnaniello, F. Donati, M. Pivetta, G. Autès, O. V. Yazyev, S. Rusponi, and H. Brune, Phys. Rev. B **91**, 235426 (2015).

[69] Note that $\Delta S_z = \pm 1, 0$ also allows the $|0\rangle \rightarrow |6\rangle$ transition. This transition has a higher energy. The fact that it is not giving a significant contribution to the dI/dV spectrum signifies that its rate is low and that the excited states are long lived such that we are not limited to transitions starting from the ground state.

[70] C. F. Hirjibehedin, C. P. Lutz, and A. J. Heinrich, Science **312**, 1021 (2006).

[71] S. Kahle, Z. Deng, N. Malinowski, C. Tonnoir, A. Forment-Aliaga, N. Thontasen, G. Rinke, D. Le, V. Turkowski, T. S. Rahman, S. Rauschenbach, M. Ternes, and K. Kern, Nano Lett. **12**, 518 (2012).